Eco-friendly photocatalysts achieved by zeolite fixing

Runyuan Ma, Liang Wang*, Sai Wang, Chengtao Wang, Feng-Shou Xiao*

Key Lab of Applied Chemistry of Zhejiang Province, Department of Chemistry, Zhejiang University, Hangzhou, 310007, PR China

ARTICLE INFO

ABSTRACT

Photocatalysts for pollutant degradation have been extensively investigated but extremely challenging for practical applications, because the radicals formed on the catalyst surface are pernicious to organisms in the nature. We develop a new concept of eco-friendly photocatalyst to impart shape-selective catalysis for pollutants removal but eco-friendly for organisms. The proof-of-concept design is demonstrated by fixing conventional photocatalysts (e.g. TiO_2, Pt/TiO_2) inside of zeolite crystals to form a pomegranate-like structure, as confirmed by electron microscopy and FTIR spectroscopy. In the photodegradation with chlorophyll molecules and grasses as model of the organisms, the zeolite-fixed photocatalysts give ideal performances for the selective degradation of pollutants but are harmless to the organisms, outperforming the conventional photocatalysts. This unique phenomenon is reasonably attributed to the shape-selectivity of the zeolite sheath with uniform micropores, where the pollutant molecules with sizes less than zeolite micropores could be diffused but bulky organisms are hindered to access to the radicals on the TiO_2 surface.

© 2017 Elsevier B.V. All rights reserved.

1. Introduction

The solar-driven photocatalytic processes, including pollutant elimination [1–7], fine chemical synthesis [8–11], and hydrogen evolution from water [12–15], have attracted much attention in the past years, because of the inexhaustible and clean features of solar energy. Particularly, the elimination of organic pollutants by photodegradation is widely investigated, which is an old but critically important story in the field of photocatalysis, because of the significant advantage of organic pollutants removal by direct transformation into carbon dioxide [1–7]. TiO_2-based catalysts have shown outstanding catalytic activity in the photodegradation of organic pollutants under ultraviolet or visible light irradiation, where an ocean of developments have been achieved [2,4–6,16–20]. However, up to date, rare of the photodegradation has been practically applied for cleaning water in nature, because the oxide radicals formed on the photocatalyst surface under solar light could degrade both the pollutants and the organisms in the nature [21–23]. Additionally, the nanosized photocatalysts, such as the well-known P25 TiO_2, are also unfavorable because these nanoparticles could enter the circulatory system of both plants and animals, thus causing additional problems [21,22]. These features

are challenging for practical applications of photocatalysts. To the best of our knowledge, an ideal eco-friendly photocatalyst, which is expected to selectively degrade the organic pollutants but be completely harmless to the organisms in nature, is still unachieved.

In this work, we have developed a strategy for synthesizing eco-friendly photocatalysts by fixing the conventional photocatalysts inside of zeolite crystals (cat@zeolite) to form a pomegranate-like structured catalyst, where the metal oxides serve as photocatalytically active sites and the zeolite micropores use as shape-selective sheath. Considering the organisms in nature have relatively bulky sizes, the zeolite sheath with micropores could prevent the access of organisms to the photocatalysts, but favors the diffusion of organic pollutant molecules smaller than zeolite micropores. As typical photocatalysts of P25 TiO_2 under ultraviolet and Pt nanoparticle-loaded P25 (Pt/TiO_2) under visible light irradiation [24–26], they are completely fixed inside of S-1 zeolite via solvent-free route [27], designated as TiO_2@S-1 and Pt/TiO_2@S-1, respectively. In the photodegradation tests in a model ecosystem, as we expected, the organism are undamaged, while the pollutants are completely degraded in these cases.

2. Experimental

2.1. Materials

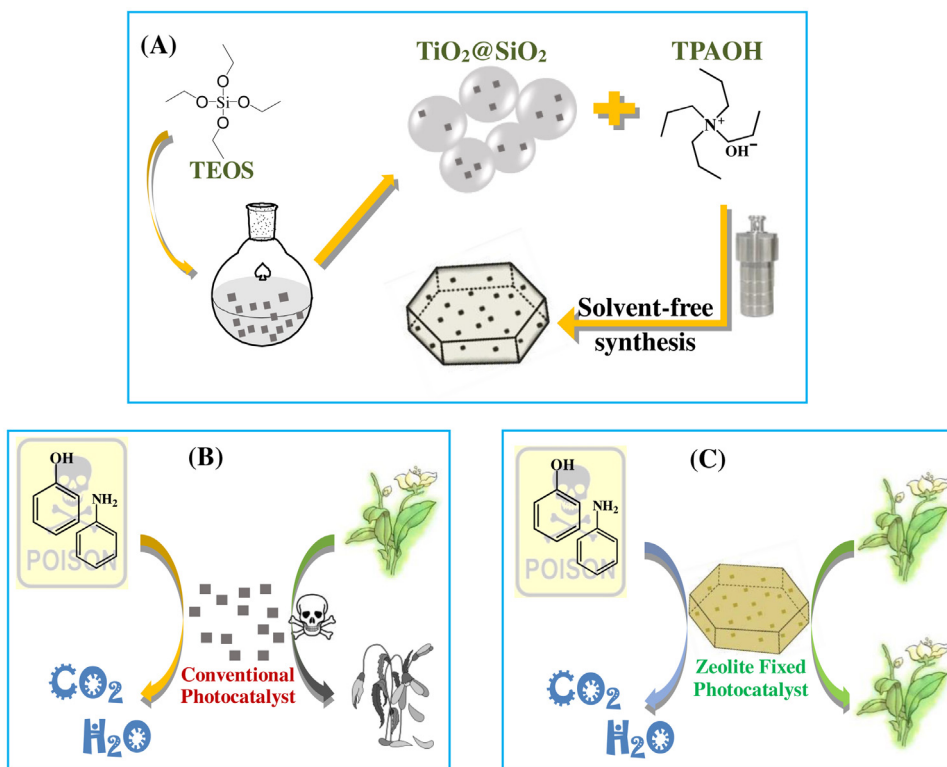Tetraethylorthosilicate (TEOS), phenol, aniline, tetrapropylammonium hydroxide (TPAOH, 40 wt%), P25, TMHP

Fig. 1. Synthesis and catalysis strategy. (A) Procedure for the synthesis of zeolite fixed photocatalyst (TiO$_2$@S-1); (B) The conventional TiO$_2$ photocatalyst is harmful to the organisms during the photodegradation of pollutants; (C) The zeolite-fixed photocatalyst is eco-friendly during the photodegradation process.

(2,2,6,6-tetramethyl-4-piperidol), nitrobenzene, and 1,3-dimethyl-5-nitrobenzene were purchased from Aladdin Company. NaOH, ammonia hydroxide, sodium aluminate, and ammonium nitrate were purchased from Tianjin Guangfu Chemical Co. Distilled water was purchased from Watsons. Ethanol (absolute) was purchased from Shanghai Lingfeng Chemical Reagent Co. H$_2$PtCl$_6$ was obtained from Zhejiang Metallurgical Research Institute. Chlorophyll was obtained from Ji'an Hai natural plant Co. Ltd. All reagents were of analytical grade and used without further purification.

2.2. Synthesis

2.2.1. Synthesis of Pt/TiO$_2$ sample

The Pt/TiO$_2$ was synthesized by impregnation method. As a typical run, the 1 g of P25 TiO$_2$ powder was dispersed in the solution of H$_2$PtCl$_6$ (20 ml of water and 8 mg of Pt), followed by ultrasonic treatment for 1 h at room temperature. After stirring at 80 °C under vacuum to remove the water, the solid was dried at 100 °C for 24 h and calcined at 400 °C for 4 h to obtain the Pt/TiO$_2$ catalyst.

2.2.2. Synthesis of SiO$_2$ capsulated TiO$_2$ (TiO$_2$@SiO$_2$)

As a typical run, 15 mg of TiO$_2$ were added into 50 ml of water and 40 ml of ethanol, followed by ultrasonic treatment for 1 h at room temperature. Then TEOS (9.5 mmol) was added under stirring, and the pH of the liquor was adjusted to ∼10 by ammonium hydroxide. After stirring at 50 °C to remove the water and ethanol under vacuum, drying at 100 °C for 12 h, the TiO$_2$@SiO$_2$ was finally obtained. The SiO$_2$ capsulated Pt/TiO$_2$ (Pt/TiO$_2$@SiO$_2$) was synthesized via the same method except using Pt/TiO$_2$ as precursor.
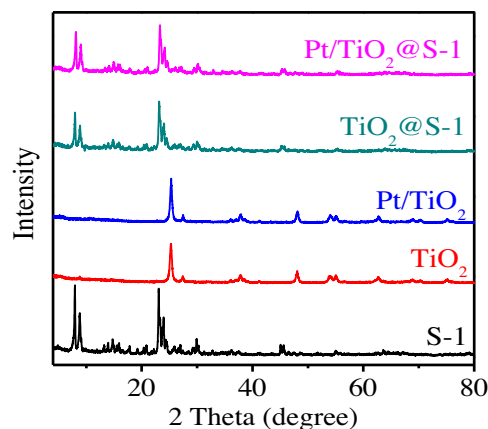

Fig. 2. XRD patterns of various samples.

2.2.3. Synthesis of TiO$_2$@S-1 and Pt/TiO$_2$@S-1 samples

As a typical run for the synthesis of TiO$_2$@S-1, 0.6 g of TiO$_2$@SiO$_2$ and 0.5 g of TPAOH (40%) were grinded at room temperature for 15 min, then the solid was dried under vacuum at room temperature for 15 min to partly remove the water. Then the solid powder was transferred into an autoclave and thermally treated at 180 °C for 5 days. After removing the organic template by calcining at 550 °C for 4 h, the TiO$_2$@S-1 sample was finally obtained. The Pt/TiO$_2$@S-1 sample was synthesized via the same method except using Pt/TiO$_2$@SiO$_2$ as precursor.

2.2.4. Synthesis of NaOH-TiO$_2$@S-1 sample

As a typical run, 1 g of TiO$_2$@S-1 was added to 50 ml of NaOH solution (2 M). After stirring at room temperature for 10 min, the
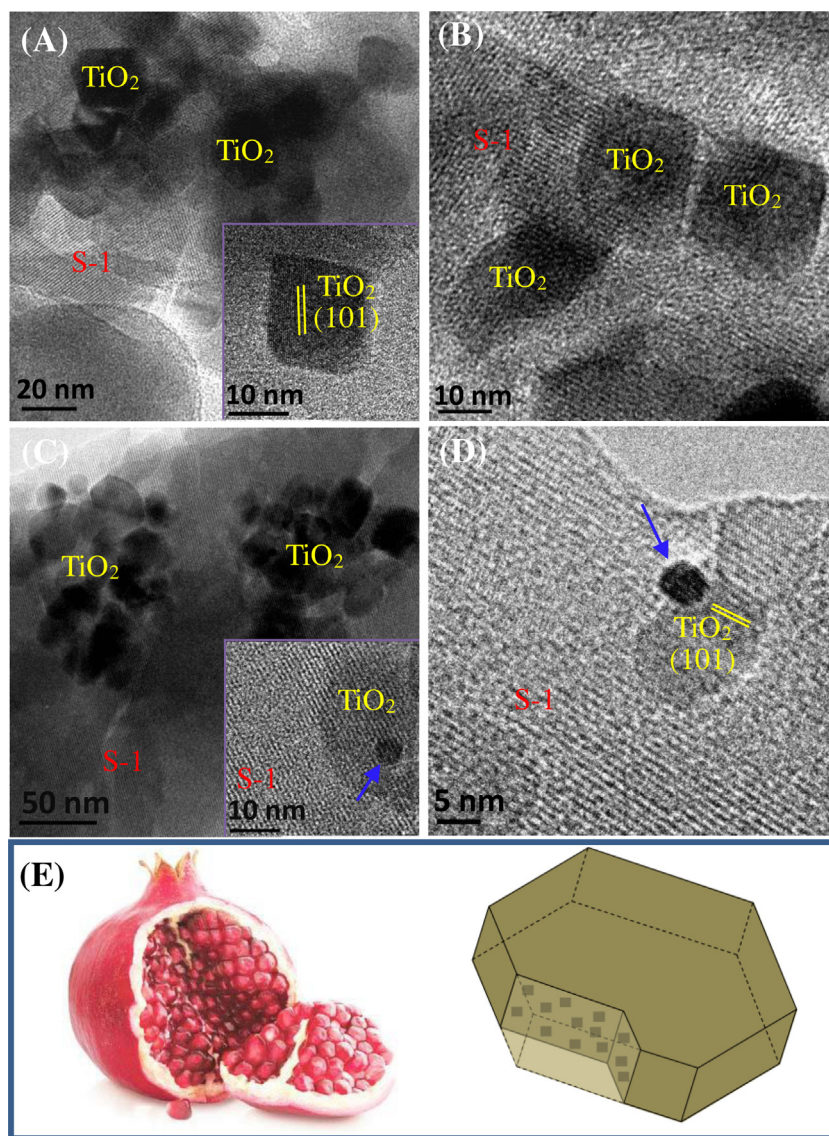
Fig. 3. TEM characterization. TEM tomographic images of (A and B) TiO$_2$@S-1 and (C and D) Pt/TiO$_2$@S-1. The blue arrows highlight the Pt nanoparticles. (E) Scheme of the pomegranate-like structure. (For interpretation of the references to colour in this figure legend, the reader is referred to the web version of this article.)

mixture was centrifuged, washed with a large amount of water, and dried at 100 °C for 12 h to obtain the NaOH-TiO$_2$@S-1 sample.

2.2.5. Synthesis of Y and TiO$_2$@Y samples

As a typical run for the synthesis of Y zeolite (H form), 3.17 g of SiO$_2$·3H$_2$O were mixed with 1.64 g of NaAlO$_2$ and grinded for 15 min at room temperature, then the mixture was transferred to an autoclave and thermally treated at 100 °C for 24 h. After washing with water and ethanol, the Na-form Y zeolite was obtained. The Na-form Y zeolite was transferred into H-form by ion-exchange and calcination. Typically, 1 g of the Na-form Y zeolite was stirred in 50 ml of ammonium nitrate solution (1 M) at 80 °C for 2 h, and the solid was filtered and calcined at 450 °C for 4 h. The above ion exchange and calcination steps were repeated to obtain the final H-from Y zeolite. The TiO$_2$@Y sample was synthesized via the same method except using TiO$_2$@SiO$_2$ as silicon source.

2.3. Catalyst characterization

Powder X-ray diffraction patterns (XRD) were obtained with a Rigaku powder X-ray diffractometer using CuKα radiation (λ = 0.1542 nm). The metal content was determined by inductively coupled plasma spectroscopy (ICP, PerkinElmer 3300DV). Nitrogen sorption isotherms were measured at −196 °C using a Micromeritics ASAP 2020 M system. The samples were degassed for 10 h at 150 °C before the measurements. Thermogravimetric (TG) curves were performed on a SDT Q600 Simultaneous DSC-TGA in flowing air with heating rate of 10 °C/min. Transmission electron microscopy (TEM) images were performed on a JEM-2100F electron microscopy (JEOL, Japan) with an acceleration voltage of 200 kV. The samples were ultrasonically dispersed in ethanol and then a drop of the solution was deposited onto a holey C/Cu grid for HAADF-STEM characterization. Scanning electron microscopy (SEM) experiments were performed with Hitachi SU-8010 electron microscopes. IR spectra were recorded using a Nicolet IS50 FT-IR spectrometer equipped with a MCT/A detector and ZeSe windows and a high temperature reaction chamber. The nitroarene stream was introduced into the system with a flow of Ar carrier gas (30 sccm) with the reactant partial pressure in the range of 10–20 mBar. The samples were treated at 300 °C for 1 h in flowing Ar before the test. The adsorption of nitroarene was tested at 50 °C. The UV–vis spectra were recorded on a Perkin-Elmer Lambda 20
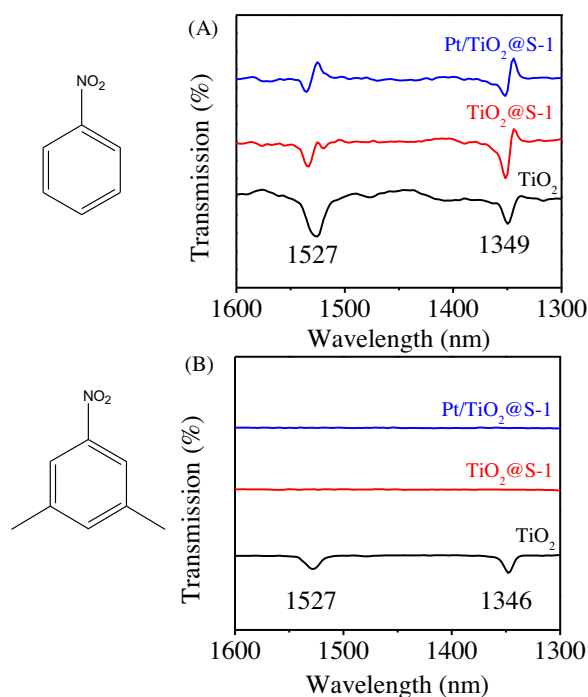
Fig. 4. FT-IR spectra of (A) nitrobenzene, (B) 1,3-dimethyl-5-nitrobenzene adsorbed on the TiO_2, TiO_2@S-1, and Pt/TiO_2@S-1 samples.

spectrometer. EPR spectra were measured on a Bruker A300 EPR Spectrometer with a digital temperature control system (Bruker ER 4131 VT). Frequency: 9.869 GHz, Attenuation: 10 dB, Modulation amplitude: 1.00 G, Time constant: 10.24 ms for all spectra. For all the samples, no saturation was observed within the range of the microwave power. The EPR spectra of the samples were measured at 291.1 K. The generation of radical species was monitored by EPR spectroscopy associated with the spin trapping technique using TMHP as superoxide radicals scavenger. As a typical run, the powders of various samples were suspended in 3 ml of TMHP solution in distilled water (50 mM), and exposed in visible light irradiation for 10 min. Then 50 μl of the liquor was transferred into quartz capillary for recording the EPR signal.

2.4. Catalytic tests

Photocatalytic degradation tests were performed in a quartz photo reactor with magnetic stirrer (900 rpm) under visible light and UV light using a 350 W xenon lamp (320–800 nm with a 400 nm filter) and 300W Hg lamp (350 nm–450 nm), respectively. The reaction temperatures were controlled to be lower than 30 °C by a flow-water cooling system. As a typical run, a certain amount of photocatalysts (10 mg of TiO_2, Pt/TiO_2, or 80 mg of zeolite fixed catalysts) were suspended in 30 ml of reaction solution containing CP (2.5 g/L) and pollutant molecules [8.3 ppm of phenol, 20 ppm (TiO_2 and TiO_2@S-1) and 100 ppm (Pt/TiO_2 and Pt/TiO_2@S-1) of aniline, or 20.8 ppm of 3,5-dimethylaniline]. Before each reaction run, the liquor was stirred for 1 h at room temperature in dark to achieve the equilibrium adsorption, following by turning on the lamp to start the reactions. After collection of 3 ml of the suspensions in photoreaction and removal of photocatalysts through syringe filters (Ø = 0.022 mm), the concentrations of phenol, aniline, and CP were calculated from the intensity of the peaks in UV–vis spectra at 270, 280, and 650 nm, respectively.

The catalytic tests in the presence of grass (ophiopogon japonicus) were performed in glass conical flask reactors. The reactors were placed in an open square for receiving sunlight irradiation in the day time, and the tests last as long as 20 days for grass experiments. 10 mg of TiO_2, Pt/TiO_2, or 80 mg of zeolite fixed catalysts were used. The pollutants were added at 10:00-11:00 in the morning. The photographs were taken at about 1:00 in the afternoon. The days during the tests are mostly sunshine with atmospheric temperature at 15–29 °C during the tests.

3. Results and discussion

In order to develop efficient photocatalysts, we employ the commercial P25 TiO_2 (particle size, ∼25 nm; Brunauer-Emmett-Teller surface area, 53 m^2/g; anatase/rutile phase ratio, 4/1) for the synthesis of TiO_2@zeolite photocatalysts. As shown in the synthesis procedure (Fig. 1A), the P25 TiO_2 was encapsulated with amorphous SiO_2 obtained from controllable hydrolysis of tetraethyl orthosilicate in nanosized TiO_2 colloid. After grinding the solid with tetrapropylammonium hydroxide (TPAOH, 40 wt%) at room temperature in air, the solid mixture was transformed into an autoclave for crystallization at 180 °C for 5 days. After washing with water, drying, and calcining at 550 °C for 4 h to remove the organic template, the TiO_2@S-1 was finally obtained. The TiO_2@S-1 sample has TiO_2 loading at 2.74 wt%, exhibiting a significant adsorption in the UV region (<400 nm). Similarly, Pt/TiO_2@S-1 sample was synthesized, giving obvious adsorption in both the UV and visible region. The Pt and TiO_2 loadings in the Pt/TiO_2@S-1 are 0.02 and 2.56 wt%, respectively (Table S1). Fig. 2 shows XRD patterns of the TiO_2@S-1 and Pt/TiO_2@S-1, giving typical peaks associated with MFI zeolite structure. Fig. S1 shows nitrogen sorption isotherms of the TiO_2@S-1 and Pt/TiO_2@S-1, displaying typical Langmuir adsorption. Correspondingly, they show high surface areas and large pore volume (418 m^2/g and 0.16 m^3/g for TiO_2@S-1 and 380 m^2/g and 0.15 m^3/g for Pt/TiO_2@S-1). In addition, the scanning electron microscopy (SEM) images of the TiO_2@S-1 and Pt/TiO_2@S-1 show uniform crystalline morphology. Notably, it is difficult to observe the peaks of TiO_2 and metallic Pt in the XRD patterns of the TiO_2@S-1 and Pt/TiO_2@S-1, which might be due to the relative low loading of TiO_2 and Pt in the samples.

Fig. 3 shows the tomogram-section TEM images of the TiO_2@S-1 and Pt/TiO_2@S-1 samples, which offer the sectioned view of the samples to avoid the influence of TiO_2 particles on the external surface. In the images of TiO_2@S-1 and Pt/TiO_2@S-1, the TiO_2 particles with obviously darker contrast than zeolite could be directly observed (Fig. 3A and B), confirming that the TiO_2 particles are indeed fixed inside of zeolite S-1 crystals [28]. Particularly, in the tomogram-section TEM image of the Pt/TiO_2@S-1, a Pt nanoparticle is observed on TiO_2, which is fixed in S-1 zeolite crystals (Fig. 3C and D). These data demonstrate that the TiO_2 or Pt/TiO_2 crystals are successfully fixed inside of the S-1 zeolite crystals to form a pomegranate-like structure with zeolite sheath (Fig. 3E).

Furthermore, the structure of TiO_2@S-1 and Pt/TiO_2@S-1 was investigated by IR spectra of probing molecules. Based on the knowledge that the nitro group has strong IR adsorption on TiO_2 [29,30], we have employed nitrobenzene and 3,5-dimethylnitrobenzene as probing molecules. Because nitrobenzene is small enough to fit the micropores of S-1 zeolite and 3,5-dimethylnitrobenzene is too large, the nitrobenzene could easily access to TiO_2 sites in the TiO_2@S-1 and Pt/TiO_2@S-1 samples, giving strong bands of nitro group at 1349 and 1527 cm^{-1}, while these bands are undetectable for 3,5-dimethylnitrobenzene (Fig. 4). In contrast, TiO_2 sample without zeolite sheath always gives these IR bands for the adsorption of both nitrobenzene and 3,5-dimethylnitrobenzene molecules. These results confirm the conclusion that the TiO_2 crystals in TiO_2@S-1 and Pt/TiO_2@S-1 are entirely occluded within the matrix of zeolite S-1 crystals, where the zeolite micropores prevented the diffusion of 3,5-
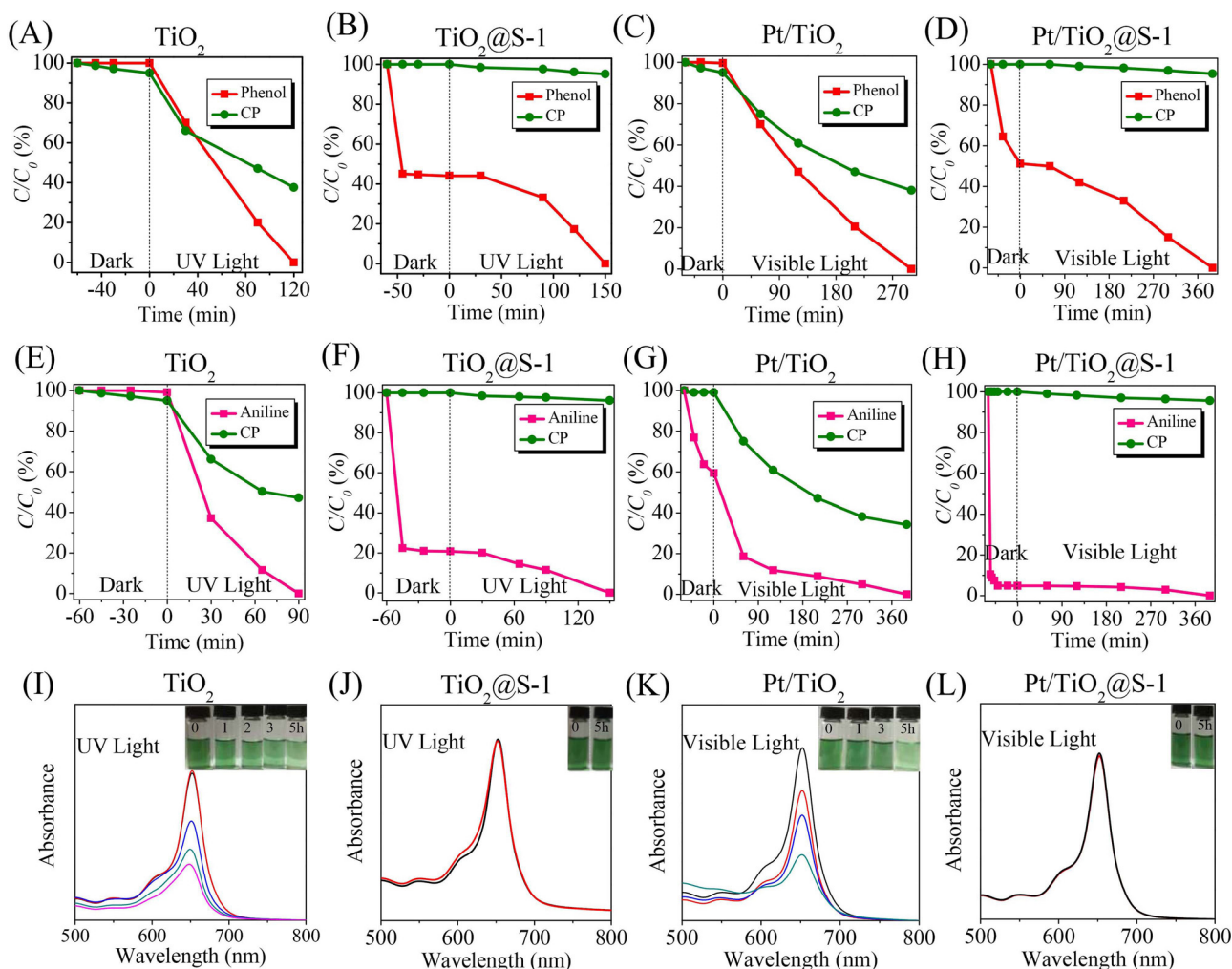
Fig. 5. Data characterizing various catalysts in the degradation reaction. (A–H) Dependences of substrate concentration on time over various catalysts in the photodegradation of phenol, aniline and chlorophyll, respectively. (I–L) UV–vis spectra of the chlorophyll solution in the 5 h degradation tests over various catalysts. Insert: the photographs of the solution during the tests. Reaction conditions: 10 mg of TiO_2, Pt/TiO_2, or 80 mg of zeolite fixed catalysts, 30 ml of reaction solution containing CP (2.5 g/L) and pollutant molecules: 8.3 ppm of phenol, 20 ppm (TiO_2 and TiO_2@S-1) and 100 ppm (Pt/TiO_2 and Pt/TiO_2@S-1) of aniline.

dimethylnitrobenzene to the TiO_2 sites—all in good agreement with the results of TEM characterization. On the basis of these data, it is reasonably expected to extend the zeolite shape-selective catalysisto TiO_2-based photocatalysts by a zeolite sheath [31–36].

Our investigation of the catalytic properties of various catalysts started with the photodegradation of phenol and aniline, which are major pollutants in water from leather industry and regarded as serious carcinogens. The S-1 zeolite micropores are large enough (~5.5 Å) for phenol and aniline diffusion. In these reactions, chlorophyll (CP) molecules were present in the liquor as a model of organisms in the system. Fig. 5 shows dependences of phenol, aniline and chlorophyll degradation on time over various TiO_2-containing catalysts. Normally, the conventional photocatalyst is non-selective and active for the degradation of most organic molecules. As a result, TiO_2 gives complete degradation of phenol and aniline pollutants in 120 and 90 min, respectively (Fig. 5A and E). At the same time, the undesirable degradation of chlorophyll always occurs, resulting in the decrease of chlorophyll concentration to less than 50% of the original values (Fig. 5A and E). These results indicate non-selective degradation of TiO_2 for the pollutants and chlorophyll. Very interestingly, the concentration of chlorophyll is basically a constant over the TiO_2@S-1 catalyst, while the phenol and aniline display a quick adsorption in dark 15 min, followed by the complete degradation under UV irradi-

ation for 150 min (Fig. 5B and F). The complete degradation is confirmed by the IR characterization. Fig. S2 shows the IR spectra of TiO_2@S-1 in photocatalytic degradation of phenol under UV light. The TiO_2@S-1 catalyst during reaction gave obvious bands at 1540 and 1468 cm^{-1}, assigning to phenol molecule. After the reaction, these bands completely disappeared because of full degradation of the phenol molecules. This conclusion is further supported by the undetectable total organic carbon (TOC) in the reaction liquor. These data indicate the superior selectivity of TiO_2@S-1 for the degradation of pollutants in the presence of chlorophyll, because the zeolite sheath prohibits the access of chlorophyll (Fig. S3) to TiO_2 nanoparticles. Notably, even under UV irradiation for a long period of 5 h, the chlorophyll concentration is still unchangeable within error over the TiO_2@S-1 (Fig. 5J). In contrast, the chlorophyll concentration remarkably decreases over the TiO_2 catalyst under the same conditions (Fig. 5I).

Furthermore, the Pt-containing catalysts were employed for improving the photoactivities under visible light (>400 nm, Figs. S4 and S5), because modification of metals (e.g. Pt) on the TiO_2 tunes the electronic structure of TiO_2 and narrows the TiO_2 band gap for visible light response [24–26]. As expected, the UV–vis spectra of Pt/TiO_2 show obvious adsorption for visible light (Figs. S4, S6 and S7). Again, the zeolite fixed catalyst (Pt/TiO_2@S-1) exhibits excellently selective degradation of phenol and aniline in the presence

of chlorophyll (Fig. 5D and H). Even if the visible irradiation is over 5 h, the chlorophyll concentration is still remained (Fig. 5L). In comparison, the Pt/TiO$_2$ catalyzed the degradation of all the molecules of phenol, aniline, and chlorophyll (Fig. 5C and G). Additionally, it is found that the Pt modification of TiO$_2$ can significantly enhance the catalytic activity in the degradation of aniline. Table S1 shows reaction rate (r) in the degradation of aniline and phenol over TiO$_2$ under UV light and Pt/TiO$_2$ under visible light, respectively. In the degradation of phenol, the reaction over TiO$_2$ is faster than that over Pt/TiO$_2$, because of the high activity of TiO$_2$ under UV light than Pt/TiO$_2$ under visible light. However, Pt/TiO$_2$ exhibits faster reaction rate than TiO$_2$ in the degradation of aniline, which is different from that in the degradation of phenol. This phenomenon is reasonably assigned to the adsorption of anilines on the Pt species, as evidenced in Fig. 5G and H. Moreover, in the degradation of phenol, the Pt/TiO$_2$ gives the reaction order for phenol at 0.31 (Fig. S8), which is lower than that of 0.78 over TiO$_2$ catalyst. This phenomenon might be related to the adsorption of phenol on the Pt sites.

Fig. 6 shows recyclable tests of the Pt/TiO$_2$@S-1 catalyst in the degradation of phenol mixed with chlorophyll under visible irradiation. After six recycles with reaction time of 360 min in each run, the catalyst still gives full conversion of phenol (Fig. S9), confirming its excellent recyclability. In order to study the activity of the Pt/TiO$_2$@S-1 before and after the recycle tests, we artificially shorted the reaction time to 270 min in each run. The used Pt/TiO$_2$@S-1 catalysts in the 7th run displayed the degradation of 80% of the phenol, which is very similar to the as-synthesized catalyst, demonstrating the good recyclability. ICP-OES data indicate
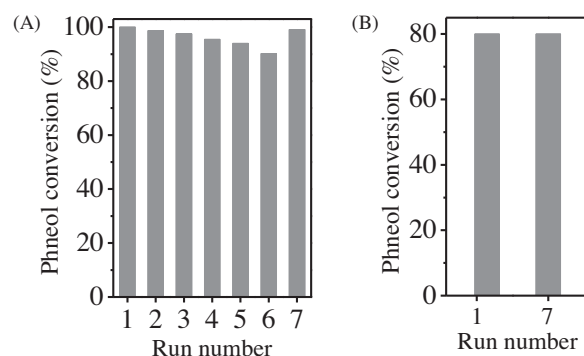

Fig. 6. Catalytic activities of the Pt/TiO$_2$@S-1 in recycling tests in the degradation of phenol for (A) 360 min and (B) 270 min in each run. After the 6th recycles, the sample was calcined and reused in the next run. The reaction conditions are the same to those in Fig. 5D.

that the Pt and Ti leaching is undetectable during the recycling tests. The unique shape-selectivity in the degradation combined with the high stability of the zeolite fixed photocatalysts offer a good opportunity to develop eco-friendly photocatalysts in the future.

Encouraged by above results, we performed the degradation of phenol and aniline pollutants in the presence of natural organisms such as grass over the Pt/TiO$_2$@S-1 photocatalyst, where the glass reactors can accept sunlight irradiation and pollutants of phenol and aniline were added periodically. The photographs in Fig. 7 show the growth of grasses over the photocatalysts of TiO$_2$, Pt/TiO$_2$, TiO$_2$@S-1 and Pt/TiO$_2$@S-1. The vitality of the grasses can be easily
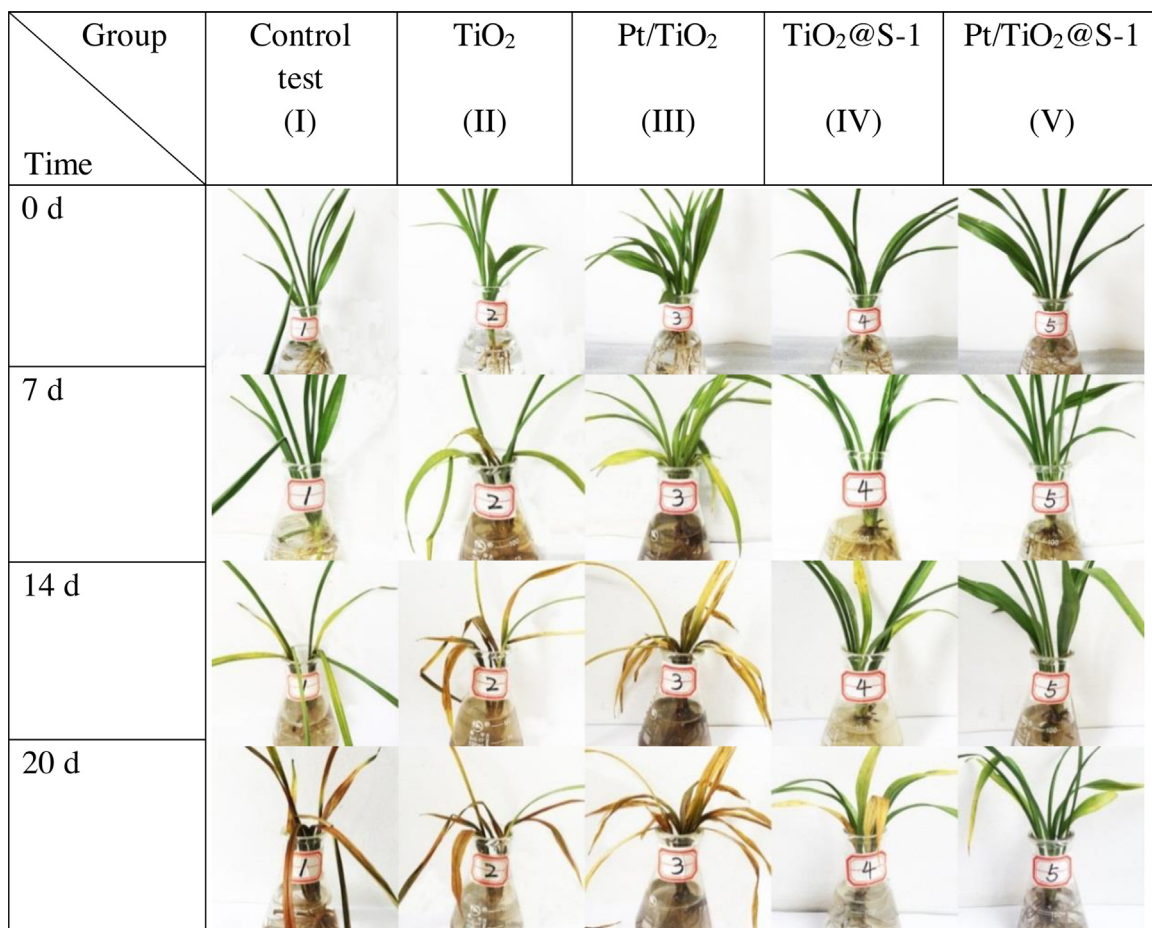

Fig. 7. Photographs of the grasses under different conditions. Adding pollutant to II–V every 2 days during the test. Adding pollutant to I every 2 days since the 7th day.
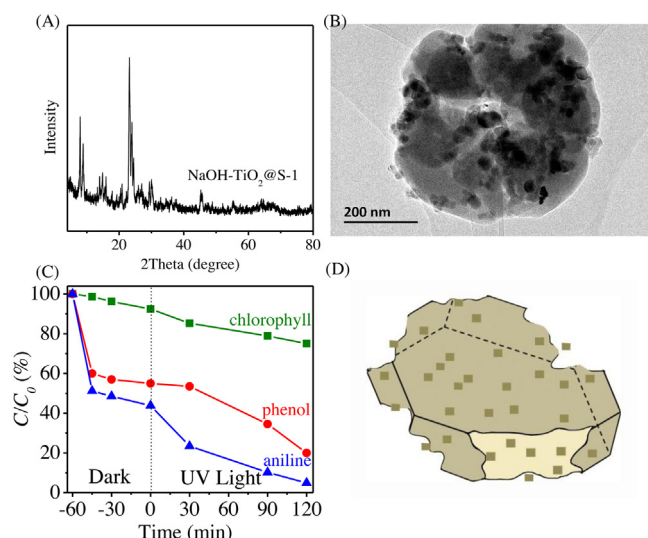
Fig. 8. (A) XRD patterns; (B) TEM image; (C) Dependences of concentration on time in the photodegradation of phenol, aniline and chlorophyll, respectively; (D) Model of NaOH-TiO₂@S-1.

observed from the color of the leaves. In the referenced experiment without any catalysts (Test I in Fig. 7), the grass leaves gradually became yellow and yellow-dark after addition of phenol and aniline. When the TiO₂ and Pt/TiO₂ were presented in the liquor (Test II and III in Fig. 7), the leaves still became yellow and yellow-dark even if the absence of any pollutants. These results demonstrate that the nanosized TiO₂ and Pt/TiO₂ photocatalysts are harmful to the grass.

It is worth noting that the grass basically kept green in the presence of phenol and aniline pollutants when the zeolite-fixed catalysts of TiO₂@S-1 and Pt/TiO₂@S-1 were added in the system (Test V and VI in Fig. 7), suggesting that the TiO₂@S-1 and Pt/TiO₂@S-1 photocatalysts might be harmless to the grass growth. To avoid the effect on individually different grasses, this kind of experiments were repeated and similar results were always achieved.

As observed in Figs. 5 and 7, the TiO₂@S-1 and Pt/TiO₂@S-1 could be regarded as eco-friendly photocatalysts with excellent selectivity for the degradation of pollutants with relatively small molecular sizes. Considering that these catalysts have the same TiO₂ nanoparticles, it is reasonably suggested that the highly selective degradation of the pollutants over the zeolite fixed catalysts should be directly attributed to the zeolite sheath rather than other factors. To confirm this idea, sodium hydroxide treatment of TiO₂@S-1 was carried out. After partial destruction of the S-1 zeolite framework in the TiO₂@S-1 (Figs. 8 A and B, S10 and Table 1), the treated sample (NaOH-TiO₂@S-1) could catalyze the degradation of both the pollutants and chlorophyll (Fig. 8C), significantly reducing the degradation selectivity, compared with the as-synthesized TiO₂@S-1. This phenomenon demonstrates the importance of the S-1 zeolite for controlling the selectivity in photodegradation over the TiO₂@S-1. After the destruction of the zeolite sheath by NaOH treatment, partial TiO₂ nanoparticles are exposed and accessible to the bulky molecules, as confirmed by the IR spectra for adsorption of nitrobenzene and 1,3-dimethyl-5-nitrobenzene (Fig. S11).

It is well known that activity of TiO₂-based photocatalysts origins from the oxide-containing radicals [37–39], which are key intermediates for the degradation. Fig. 9 shows the electron paramagnetic resonance (EPR) spectra of various samples under solar irradiation with 2,2,6,6-tetramethyl-4-piperidinol (TMHP) for capturing the radicals. Notably, strong signals associated with superoxide radicals appeared at the EPR spectra of TiO₂ and Pt/TiO₂
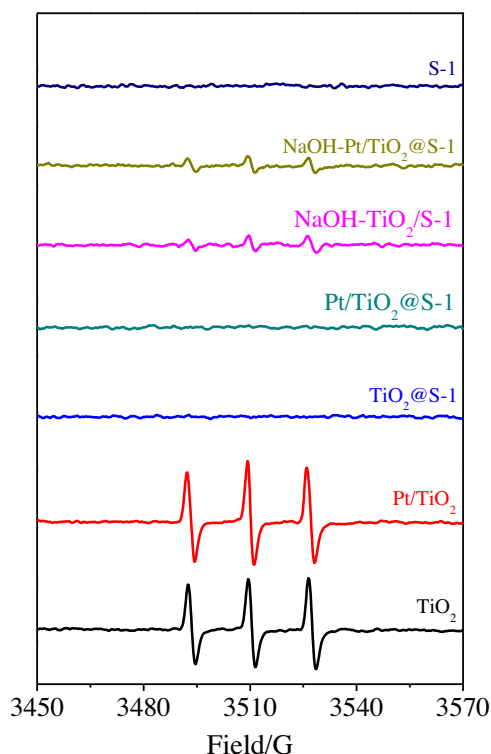

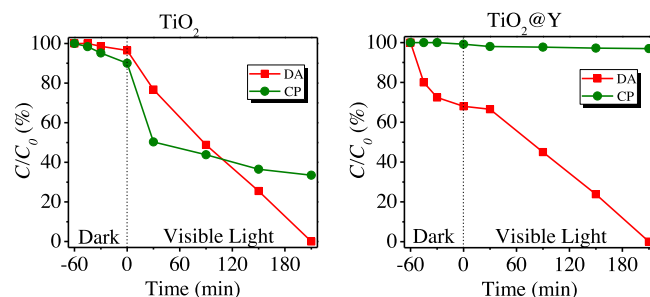**Fig. 9.** EPR spectra of various samples with TMHP as radical capture.

Fig. 10. Data of TiO₂ and TiO₂@Y in the photocatalytic degradation reaction. Dependences of concentration change on time over various catalysts in the photo degradation of aniline derivatives (3,5-dimethylaniline, DA) and chlorophyll (CP).

[40–42]. On the contrary, these signals are completely absent in the EPR spectra of TiO₂@S-1 and Pt/TiO₂@S-1. This phenomenon is interpreted by that the TMHP molecules larger than the micropores of S-1 zeolite cannot capture the radicals formed on the surface of TiO₂ inside of S-1 zeolite crystals. However, when the S-1 zeolite sheath was partially destroyed by the NaOH treatment, the NaOH-TiO₂@S-1 exhibited weak signals associated with superoxide radicals, indicating the importance of the S-1 zeolite sheath for isolation of the radicals.

Moreover, the concept of fixing the TiO₂-based photocatalysts into zeolite crystals could be extended to the use of various zeolites. For example, when Y zeolite with larger micropores (∼0.68 nm) was employed as the zeolite sheath, the Y zeolite fixed TiO₂ catalyst (TiO₂@Y, Figs. S12–S15) could be prepared [43]. The TiO₂@Y photocatalyst shows full degradation of substituted aniline with larger sizes than phenol and aniline under photocatalytic conditions, because the micropores of zeolite Y are large enough for diffusion of these substituted aniline. Very similarly, this photocatalyst is also eco-friendly to the chlorophyll molecule (Fig. 10).

Table 1
The textual parameters of various samples.

Entry	Catalyst	S_{BET}[a] ($m^2\,g^{-1}$)	V_p[a] ($cm^3\,g^{-1}$)	TiO_2 loading (wt%)[b]	Pt loading (wt%)[b]
1	S-1	450	0.18	–	–
2	TiO_2@S-1	418	0.16	2.74	–
3	Pt/TiO_2@S-1	380	0.15	2.56	0.02
4	NaOH–TiO_2@S-1	266	0.16	3.26	–

[a] By N_2 sorption test.
[b] By ICP-OES analysis.

4. Conclusion

In summary, we demonstrate a novel type of eco-friendly photocatalysts achieved by fixing the conventional TiO_2-based photocatalysts inside of zeolite crystals. The S-1 zeolite fixed TiO_2 (TiO_2@S-1) and Pt/TiO_2 (Pt/TiO_2@S-1) catalysts exhibited not only excellent shape selectivity for pollutant degradation but also eco-friendly for the model organism in a mixture of pollutants and chlorophyll due to the presence of zeolite sheath. The strategy by fixing photocatalysts inside of zeolite crystals might open a way to synthesize new generation of photocatalysts in the future.

Acknowledgment

Appendix A. Supplementary data

Supplementary data associated with this article can be found, in the online version, at http://dx.doi.org/10.1016/j.apcatb.2017.04.071.

References

[1] J.Y. Shi, Y. Kuwahara, T.C. An, H. Yamashita, Catal. Today 281 (2017) 21–28.
[2] M. Zhang, W. Jiang, D. Liu, J. Wang, Y. Liu, Y. Zhu, Y. Zhu, Appl. Catal. B 183 (2016) 263–268.
[3] Y.J. Cui, Z.X. Ding, P. Liu, M. Antonietti, X.Z. Fu, X.C. Wang, Phys. Chem. Chem. Phys. 14 (2012) 1455–1462.
[4] H. Yamashita, Y. Ichihashi, M. Harada, G. Stewart, M.A. Fox, M. Anpo, J. Catal. 158 (1996) 97–101.
[5] J. Zhang, Q. Xu, Z.C. Feng, M.J. Li, C. Li, Angew. Chem. Int. Ed. 47 (2008) 1766–1769.
[6] H. Zhang, X.J. Lv, Y.M. Li, Y. Wang, J.H. Li, ACS Nano 4 (2010) 380–386.
[7] H. Yamashita, M. Honda, M. Harada, Y. Ichihashi, M. Anpo, J. Phys. Chem. B 102 (1998) 10707–10711.
[8] X.J. Lang, X.D. Chen, J.C. Zhao, Chem. Soc. Rev. 43 (2014) 473–486.
[9] H.F. Cheng, X.F. Qian, Y. Kuwahara, K. Mori, H. Yamashita, Adv. Mater. 27 (2015) 4616–4621.
[10] W.Q. Fan, Q.H. Zhang, Y. Wang, Phys. Chem. Chem. Phys. 15 (2013) 2632–2649.
[11] Q.G. Zhai, S.J. Xie, W.Q. Fan, Q.H. Zhang, Y. Wang, W.P. Deng, Y. Wang, Angew. Chem. Int. Ed. 52 (2013) 5776–5779.
[12] Y. Ma, X.L. Wang, Y.S. Jia, X.B. Chen, H.X. Han, C. Li, Chem. Rev. 114 (2014) 9987–10043.
[13] K. Maeda, T. Takata, M. Hara, N. Saito, Y. Inoue, H. Kobayashi, K. Domen, J. Am. Chem. Soc. 127 (2005) 8286–8287.
[14] Z.G. Zou, J.H. Ye, K. Sayama, H. Arakawa, Nature 414 (2001) 625–627.
[15] Z.G. Yi, J.H. Ye, N. Kikugawa, T. Kako, S.X. Ouyang, H. Stuart-Williams, H. Yang, J.Y. Cao, W.J. Luo, Z.S. Li, Nat. Mater. 9 (2010) 559–564.
[16] A.W. Xu, Y. Gao, H.Q. Liu, J. Catal. 207 (2002) 151–157.
[17] C.H. Li, C. Koenigsmann, W.D. Ding, B. Rudshteyn, K.R. Yang, K.P. Regan, S.J. Konezny, V.S. Batista, G.W. Brudvig, C.A. Schmuttenmaer, J.-H. Kim, J. Am. Chem. Soc. 137 (2015) 1520–1529.
[18] J.H. Clark, M.S. Dyer, R.G. Palgrave, C.P. Ireland, J.R. Darwent, J.B. Claridge, M.J. Rosseinsky, J. Am. Chem. Soc. 133 (2011) 1016–1032.
[19] F.X.L.I. Xamena, P. Calza, C. Lamberti, C. Prestipino, A. Damin, S. Bordiga, E. Pelizzetti, A. Zecchina, J. Am. Chem. Soc. 125 (2003) 2264–2271.
[20] C. Ingrid, L. Stefano, F. Silvia, G. Elio, F. Bice, F. Ivana, J. Mater. Chem. 22 (2012) 19105–19112.
[21] L. Stefano, C. Ingrid, C.P. Maria, C. Giacomo, G. Elio, F. Bice, F. Ivana, Chem. Commun. 46 (2010) 8478–8480.
[22] A. Noureddine, C. Luis, H. Eric, ACS Appl. Mater. Interfaces 1 (2009) 2141–2146.
[23] R. Olivier, V.S. Muthukonda, K.-L.D. Maithaa, S. Loïc, K. Nicolas, K. Valérie, J. Catal. 269 (2010) 179–190.
[24] S. Bai, L. Yang, C.L. Wang, Y. Lin, J.L. Lu, J. Jiang, Y.J. Xiong, Angew. Chem. Int. Ed. 54 (2015) 14810–14814.
[25] C.B. Zhang, F.D. Liu, Y.P. Zhai, H. Ariga, N. Yi, Y.C. Liu, A. Kiyotaka, F.-S. Maria, H. He, Angew. Chem. Int. Ed. 51 (2012) 9628–9632.
[26] N. Zhang, S.Q. Liu, X.Z. Fu, Y.-J. Xu, J. Phys. Chem. C 115 (2011) 9136–9145.
[27] C.T. Wang, L. Wang, J. Zhang, H. Wang, J.P. Lewis, F.-S. Xiao, J. Am. Chem. Soc. 138 (2016) 7880–7883.
[28] L. Zhang, S.Z. Qiao, Y.G. Jin, H.G. Yang, S. Budihartono, F. Stahr, Z.F. Yan, X.L. Wang, Z.P. Hao, G.Q. Lu, Adv. Funct. Mater. 18 (2008) 3203–3212.
[29] L. Wang, J. Zhang, H. Wang, Y. Shao, X.H. Liu, Y.-Q. Wang, J.P. Lewis, F.-S. Xiao, ACS Catal. 6 (2016) 4110–4116.
[30] S. Yasuhiro, H. Hiroaki, T. Yoshiki, Y. Sugano, S. Ichikawa, T. Hirai, ACS Catal. 3 (2013) 2318–2326.
[31] A. Corma, V. Fornes, S.B. Pergher, T.L.M. Maesen, J.G. Buglass, Nature 396 (1998) 353–356.
[32] A.D. Schmitz, G. Bowers, C.S. Song, Catal. Today 31 (1996) 45–46.
[33] S.M. Csicsery, Zeolites 4 (1984) 202–213.
[34] K. Lee, S.H. Cha, S.B. Hong, ACS Catal. 6 (2016) 3870–3874.
[35] F.-K. Shieh, S.-C. Wang, C.-I. Yen, C.-C. Wu, S. Dutta, L.-Y. Chou, J.V. Morabito, P. Hu, M.-H. Hsu, K.C.-W. Wu, C.-K. Tsung, J. Am. Chem. Soc. 137 (2015) 276–279.
[36] T.-L. Cui, W.-Y. Ke, W.-B. Zhang, X.-H. Li, J.-S. Chen, Angew. Chem. Int. Ed. 55 (2016) 9178–9182.
[37] W.Y. Teoh, J.A. Scott, R. Amal, J. Phys. Chem. Lett. 3 (2012) 629–639.
[38] G. Saji, P. Suman, Z.X. Ji, B.L. Henderson, T. Xia, L.J. Li, J.I. Zink, A.E. Nel, L. Mädler, J. Am. Chem. Soc. 133 (2011) 11270–11278.
[39] M. Zhang, C.C. Chen, W.H. Ma, J.C. Zhao, Angew. Chem. Int. Ed. 47 (2008) 9730–9733.
[40] T. Hirakawa, Y. Nosaka, J. Phys. Chem. C 112 (2008) 15818–15823.
[41] R. Cai, Y. Kubota, A. Fujishima, J. Catal. 219 (2003) 214–218.
[42] R. Tijana, E.O. Agnes, I.M. Olga, M.T. David, C.T. Marion, J. Phys. Chem. 100 (1996) 4538–4545.
[43] C. Martinez-Macias, P.H. Xu, S.-J. Hwang, J. Lu, C.-Y. Chen, N.D. Browning, B.C. Gates, ACS Catal. 4 (2014) 2662–2666.